

## Electronic Supplementary Information

### **Is iron nitride or carbide highly active for oxygen reduction reaction in acidic medium?**

*Tao Sun,<sup>#</sup> Yufei Jiang,<sup>#</sup> Qiang Wu,<sup>\*</sup> Lingyu Du, Zhiqi Zhang, Lijun Yang,<sup>\*</sup> Xizhang Wang, and Zheng Hu<sup>\*</sup>*

<sup>#</sup> T. Sun and Y. F. Jiang are equally to this work

<sup>\*</sup> Corresponding authors: wqchem@nju.edu.cn (Q. W.); lijunyang@nju.edu.cn (L. J. Y.); zhenghu@nju.edu.cn (Z. H.)

#### **Content:**

#### **Experimental Section**

**ESI-1. Characterizations of NCNC and CNC**

**ESI-2. Characterizations of Fe<sub>2</sub>N/NCNC and Fe<sub>2</sub>N/CNC as-prepared and after removing Fe<sub>2</sub>N nanoparticles**

**ESI-3. Additional electrochemical characterizations of Fe<sub>2</sub>N/NCNC and Fe<sub>2</sub>N/CNC as-prepared and after removing Fe<sub>2</sub>N nanoparticles**

**ESI-4. Fe-N<sub>x</sub>/C moieties couldn't be formed in Fe<sub>2</sub>N/CNC by the same method to prepare Fe<sub>2</sub>N/NCNC**

**ESI-5. Additional characterizations of the Fe<sub>3</sub>C-based electrocatalysts**

**ESI-6. Details in theoretical calculations**

**ESI-7. The ORR process on the Fe-N<sub>4</sub>/C, Fe<sub>2</sub>N and Fe<sub>3</sub>C models**

**ESI-8. The theoretical ORR overpotentials of Fe-N<sub>4</sub>/C and Fe<sub>2</sub>N**

#### **References**

## Experimental Section

### NCNC and CNC support:

NCNC (CNC) was synthesized by the in situ MgO template method with pyridine (benzene) precursor.<sup>1</sup> In a typical procedure, basic magnesium carbonate ( $4\text{MgCO}_3 \cdot \text{Mg}(\text{OH})_2 \cdot 5\text{H}_2\text{O}$ , 1.5 g) was spread in a horizontal quartz tube of 30 mm in diameter, which was then put into a tubular furnace. When the furnace was ramped to the 700 °C at a rate of 10 °C min<sup>-1</sup> in argon, pyridine (0.4 mL) (benzene 0.7 mL) was introduced into the quartz tube within 30 min by a syringe pump. The reaction system was then cooled to ambient temperature in argon. The as-prepared sample was treated with 1:1 hydrochloric acid solution and repeatedly flushed with deionized water for the removal of the MgO template, finally drying at 60 °C for 12 h.

### Fe<sub>2</sub>N Electrocatalysts:

Fe<sub>2</sub>N/NCNC catalyst was synthesized by a convenient impregnation and nitridation method. 50 mg NCNC was dispersed ultrasonically into deionized water, and then 17.9 mg iron dichloride tetrahydrate ( $\text{FeCl}_2 \cdot 4\text{H}_2\text{O}$ ) was dissolved under stirring. After dried at 70 °C, the powder was placed into a tubular furnace for nitridation. Under NH<sub>3</sub> flow of 50 standard cubic centimeter per minute (sccm), the sample was heated to 350 °C at a rate of 5 °C min<sup>-1</sup>, then to 700 °C at 2.5 °C min<sup>-1</sup> and kept there for 3 h, finally cooled down to room temperature.

Fe<sub>2</sub>N/CNC was obtained in the same way by replacing NCNC with CNC.

For comparison, CNC-NH<sub>3</sub> catalyst was obtained by treating CNC in NH<sub>3</sub> at 700 °C for 3 h.

### Fe<sub>3</sub>C Electrocatalysts:

Fe<sub>3</sub>C-N/CNC catalyst was synthesized by carbonization method. Typically, 1.0 g polymethylmethacrylate (PMMA, MW= 35,000) was dissolved into 50 ml acetone ( $\text{CH}_3\text{COCH}_3$ ). Then, 0.3 g cyanamide ( $\text{CH}_2\text{N}_2$ ), 60 mg  $\text{FeCl}_2 \cdot 4\text{H}_2\text{O}$ , 50 mg CNC were added into the mixture and stirred for 12 h. After dried at 40 °C, the powder were placed into a tubular furnace for carbonization. Under Ar flow of 100 sccm, the sample was heated to 800 °C at a rate of 10 °C min<sup>-1</sup> and kept there for 2 h, then cooled down to room temperature.

Fe<sub>3</sub>C/CNC was obtained in the similar way but without using the nitrogen source of cyanamide.

For comparison, N/CNC and PMMA/CNC catalysts were also prepared in the similar way. The difference is that iron salt was not used for N/CNC, iron salt and cyanamide (nitrogen source) were not used for PMMA/CNC.

**Note:** For comparison, Fe<sub>2</sub>N or Fe<sub>3</sub>C nanoparticles in Fe<sub>2</sub>N- or Fe<sub>3</sub>C-based catalysts were removed by acid leaching. The leaching experiments were performed in 0.5 mol L<sup>-1</sup> H<sub>2</sub>SO<sub>4</sub> at 80 °C for 24 h, then washed and dried.

**Characterizations:** The samples were characterized by X-ray diffraction (XRD, Bruker D8 ADVANCE A25, Co K $\alpha$  radiation), transmission electron microscopy (TEM, JEM-2100, 200 kV), energy dispersive X-ray spectroscopy (EDS, SHIMADZU-SEDX), and X-ray photoelectron spectroscopy (XPS, VG ESCALAB MKII). The binding energies of XPS spectra refer to C1s at 284.6 eV. The specific surface area and pore volume were measured by using Thermo Fisher Scientific Surfer Gas Adsorption Porosimeter at 77 K with N<sub>2</sub> as adsorbate.

**Electrochemical Measurements:** The electrochemical tests including CV, RDE and RRDE were performed on a MSR electrode rotator (Pine Instrument Co.) coupled with a CHI 760C workstation (CH Instruments) with the counter electrode of Pt wire and the reference electrode of Ag/AgCl (3 mol L<sup>-1</sup> KCl). Briefly, the catalyst ink was prepared by adding certain amount of the catalyst to a mixture of 0.80 mL of water, 0.20 mL of ethanol and 40  $\mu\text{L}$  of Nafion (Dupont®, 5 wt%) with 1 h ultrasonic treatment. 10  $\mu\text{L}$  of fresh catalyst ink was dropped onto a glassy carbon electrode (GC, 0.196 cm<sup>2</sup>, Pine Instrument Co.), and dried at room temperature for 12 h. The CV, RDE and RRDE curves were recorded in O<sub>2</sub>-saturated 0.5 mol L<sup>-1</sup> H<sub>2</sub>SO<sub>4</sub> at a scan rate of 10 mV s<sup>-1</sup>. The electron transfer number ( $n$ ) and the corresponding H<sub>2</sub>O<sub>2</sub> yield were calculated by  $n=4I_{\text{disk}}/(I_{\text{disk}}+I_{\text{ring}}/N)$  and  $\text{H}_2\text{O}_2$  (%)=(200 $I_{\text{ring}}/N)/(I_{\text{disk}}+I_{\text{ring}}/N)$ ,

where  $I_{disk}$  and  $I_{ring}$  were the disk electrode current and ring electrode current, respectively. Pt ring electrode is polarized at 1.0 V vs. Ag/AgCl, and  $N$  is the collection efficiency at the ring electrode ( $N=0.26$ ).

The catalyst loading on electrode is  $0.098 \text{ mg cm}^{-2}$  for  $\text{Fe}_2\text{N}$ -based catalysts, and  $0.400 \text{ mg cm}^{-2}$  for  $\text{Fe}_3\text{C}$ -based catalysts.

## ESI-1. Characterizations of NCNC and CNC

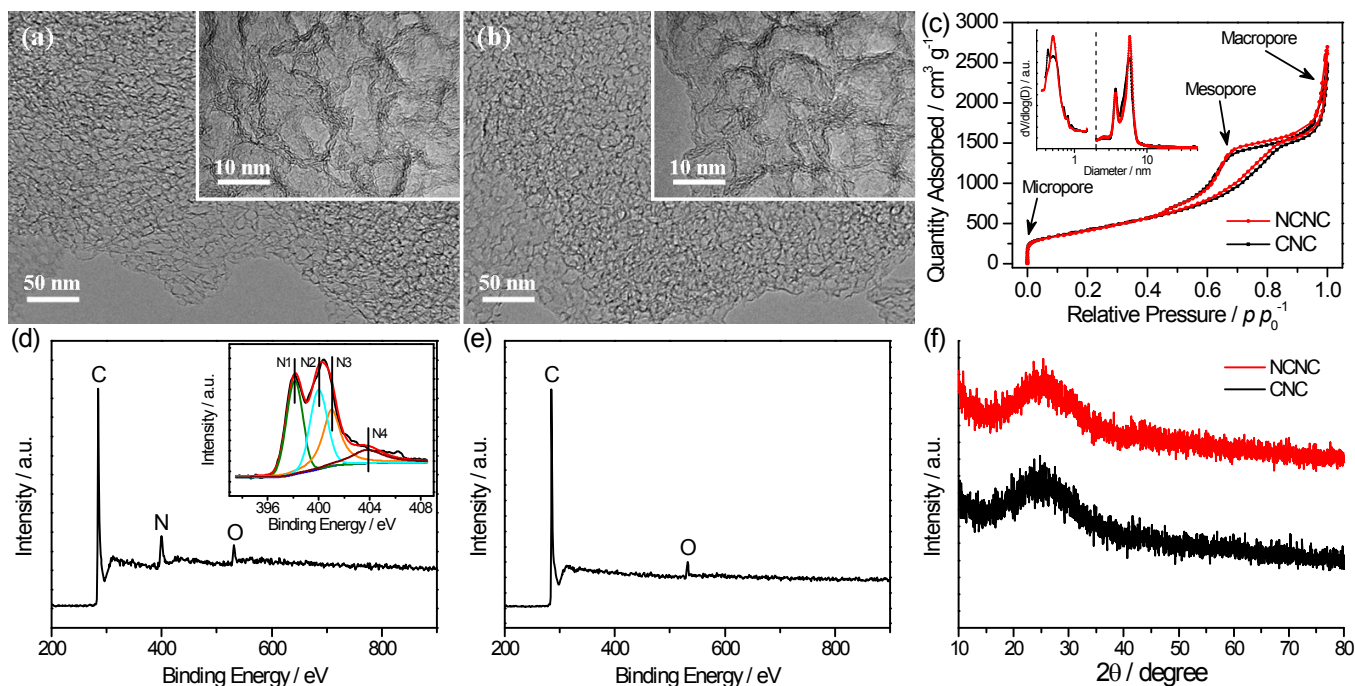


**Figure S1.** TEM and HRTEM images of (a) NCNC, and (b) CNC. (c)  $N_2$  adsorption-desorption isotherms and pore size distributions. (d,e) Survey XPS spectra of NCNC and CNC, respectively. (f) XRD patterns. Note: Inset in (d) is the corresponding N 1s spectrum.

NCNC and CNC were prepared at 700 °C by *in situ* MgO template method,<sup>1</sup> which are composed of interconnected hollow nanocages of 10-20 nm in size, with the specific surface area of 1477 and 1501 m<sup>2</sup> g<sup>-1</sup>, respectively (Figure S1a,b).  $N_2$  adsorption-desorption isotherms exhibit a typical IV-type curve with two steep uptakes ( $p/p_0 < 0.01$ ,  $p/p_0 > 0.97$ ) and a hysteresis loop ( $0.40 < p/p_0 < 0.90$ ), indicating the coexistence of micropores (< 2 nm), mesopores (2-50 nm) and macropores (> 50 nm) (Figure S1c). The nitrogen content of NCNC is ~11.4 at%, existing as pyridinic N (N1) (398.1 eV), pyrrolic N (N2) (400.0 eV), graphitic N (N3) (401.0 eV) and pyridine-N-oxide groups (N4) (403.8 eV) (Figure S1d).<sup>1</sup>

## ESI-2. Characterizations of Fe<sub>2</sub>N/NCNC and Fe<sub>2</sub>N/CNC as-prepared and after removing Fe<sub>2</sub>N nanoparticles

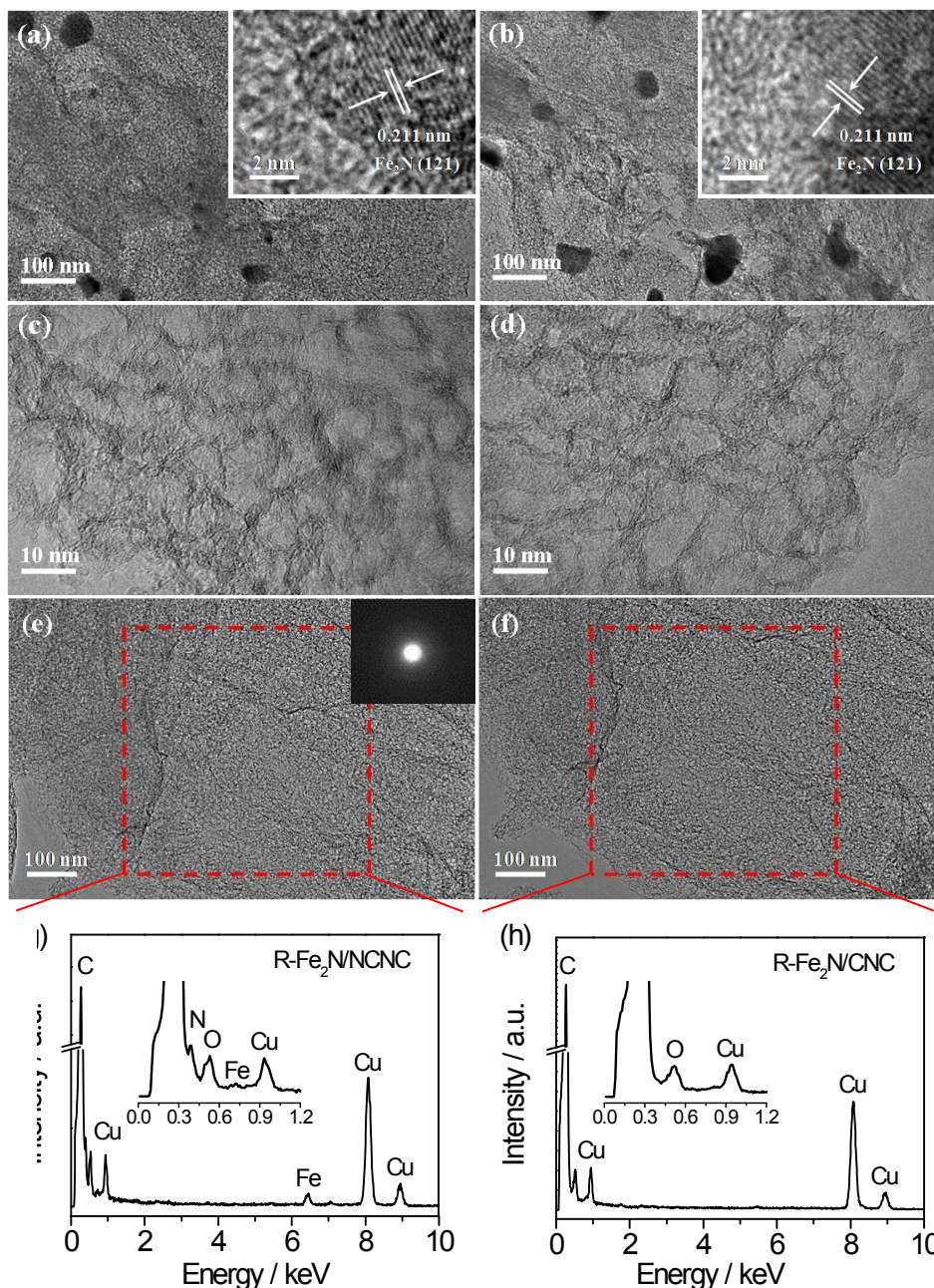


**Figure S2.** (a-f) TEM images of Fe<sub>2</sub>N/NCNC (a), Fe<sub>2</sub>N/CNC (b), R-Fe<sub>2</sub>N/NCNC (c, e), and R-Fe<sub>2</sub>N/CNC (d, f). (g, h) EDS spectra taken from the enclosed areas in (e, f), respectively. Note: These two EDS spectra are also shown in the main text of Figure 3a,b.

The as-prepared catalysts contain the Fe<sub>2</sub>N particles of 20–100 nm in size (Figure S2a,b), and the (121) planes for Fe<sub>2</sub>N are also observed, besides the (021) planes shown in Figure 1a,b. These nanoparticles can be removed by 0.5 mol L<sup>-1</sup> H<sub>2</sub>SO<sub>4</sub> leaching as shown in Figure S2c-f. EDS spectra show that Fe species is absent in R-Fe<sub>2</sub>N/CNC (Figure S2h) while still present in R-Fe<sub>2</sub>N/NCNC (Figure S2g) after removing Fe<sub>2</sub>N species. Selected area electron diffraction (SAED) result (inset in Figure S2e) indicates that no crystalline phase exists in R-Fe<sub>2</sub>N/NCNC though the Fe species is present.

**ESI-3. Additional electrochemical characterizations of Fe<sub>2</sub>N/NCNC and Fe<sub>2</sub>N/CNC as-prepared and after removing Fe<sub>2</sub>N nanoparticles**

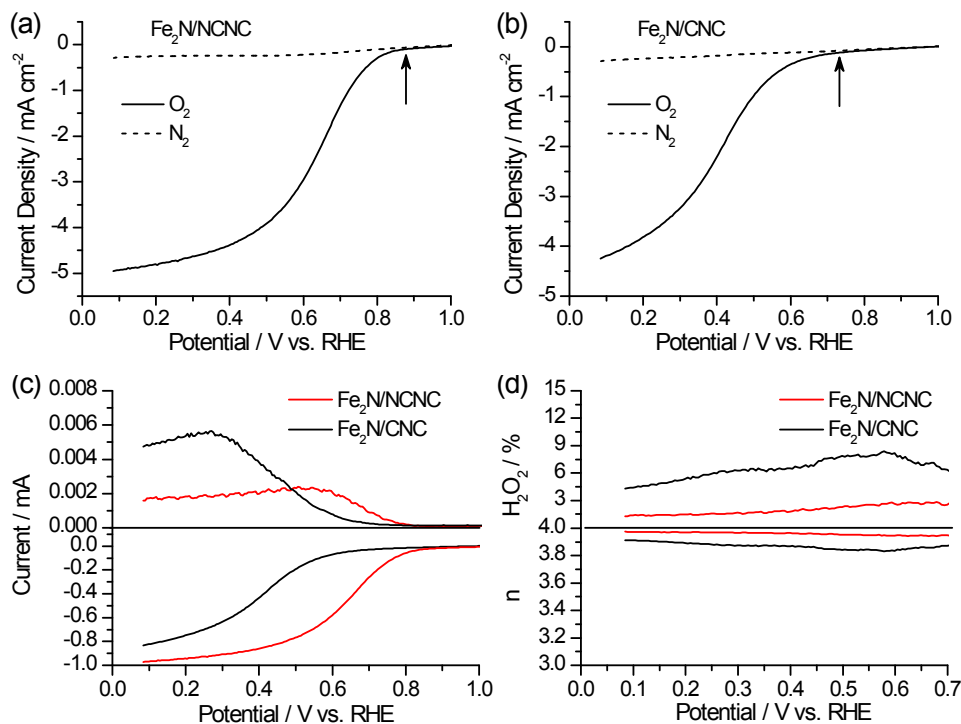


**Figure S3.** (a,b) RDE curves in O<sub>2</sub>- and N<sub>2</sub>-saturated solution. (c) RRDE curves. (d) Electron transfer number ( $n$ ) and H<sub>2</sub>O<sub>2</sub> yield vs potential.

**Table S1.** ORR activities of Fe<sub>2</sub>N/NCNC and Fe<sub>2</sub>N/CNC as-prepared and after removing Fe<sub>2</sub>N nanoparticles

Catalyst	Onset Potential (V vs. RHE)		Decrease (mV)	Current Density at 0.2 V (mA cm <sup>-2</sup> )		Decrease (mA cm <sup>-2</sup> )
	as-prepared	after		as-prepared	after	
Fe <sub>2</sub> N/NCNC	0.879	0.839	40	-4.80	-4.52	0.28
Fe <sub>2</sub> N/CNC	0.729	0.563	166	-3.82	-2.61	1.21

The onset potential ( $E_{on}$ ), defined as the separating point of RDE curves measured in O<sub>2</sub>- and N<sub>2</sub>-saturated solutions, are presented in Table S1 (Figure 2b, Figure S3a,b). Electron transfer number ( $n$ ) and corresponding H<sub>2</sub>O<sub>2</sub> yield at different potentials were obtained from RRDE curves, which indicates a dominant 4e<sup>-</sup> process for the two catalysts (Figure S3c,d).

#### ESI-4. Fe-N<sub>x</sub>/C moieties couldn't be formed in Fe<sub>2</sub>N/CNC by the same method to prepare Fe<sub>2</sub>N/NCNC

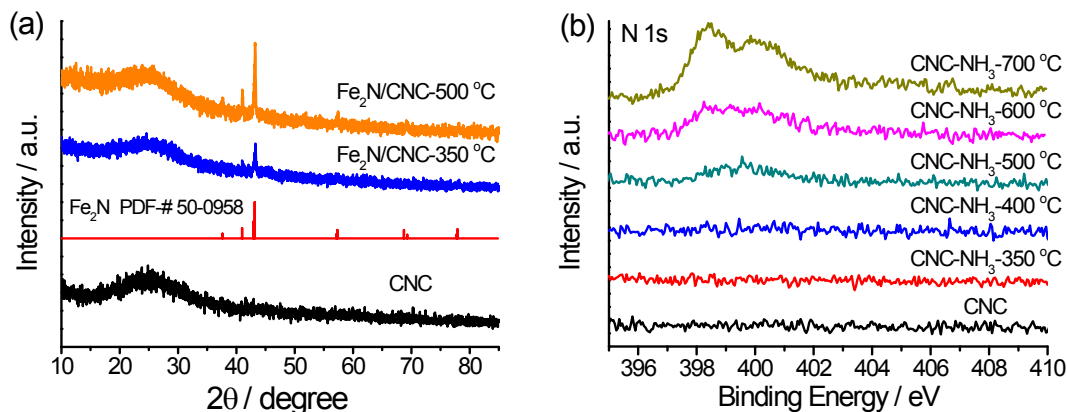


**Figure S4.** (a) XRD patterns of Fe<sub>2</sub>N/CNC prepared at different temperatures. (b) N1s XPS spectra of NH<sub>3</sub>-treated CNC at different temperatures.

It is seen that Fe<sub>2</sub>N phase is well formed by NH<sub>3</sub> treatment at 350 °C (Figure S4a), while the nitrogen-doping into CNC can occur by NH<sub>3</sub> treatment of CNC at least over 500 °C (Figure S4b).

In the preparation of Fe<sub>2</sub>N/NCNC, Fe source (from FeCl<sub>2</sub>), N and C sources from NCNC support coexisted at the very beginning. Hence, during annealing the coexisting mixture in NH<sub>3</sub> above 350 °C to prepare Fe<sub>2</sub>N phase, Fe-N<sub>x</sub>/C moieties could be formed simultaneously. Actually, this process is similar to the common case to prepare Fe-N<sub>x</sub>/C catalyst by annealing the coexisting Fe, N and C sources.<sup>2</sup>

In contrast, in the preparation of Fe<sub>2</sub>N/CNC, annealing the coexisting mixture of Fe source (from FeCl<sub>2</sub>) and CNC support in NH<sub>3</sub> at 350 °C or below 500 °C could form Fe<sub>2</sub>N phase only, and Fe-N<sub>x</sub>/C moieties couldn't be formed, due to the absent C-N bonding in the support which could be formed at least over 500 °C (see Figure S4b). When the annealing temperature was over 500 °C, Fe source from FeCl<sub>2</sub> was little left which was consumed by forming the stable Fe<sub>2</sub>N phase below 500 °C. Hence, Fe-N<sub>x</sub>/C moieties could also not be formed.

Based on the preceding experimental data and analysis, we could fully understand the relationship of the activities of all the species in Figure 2. The activity of R-Fe<sub>2</sub>N/CNC catalyst is very close to that of the NCNC or NH<sub>3</sub>-treated CNC, since nitrogen doping into the CNC support happened during preparing the Fe<sub>2</sub>N/CNC catalyst at 700 °C (Figure S4b).

### ESI-5. Additional characterizations of the Fe<sub>3</sub>C-based electrocatalysts

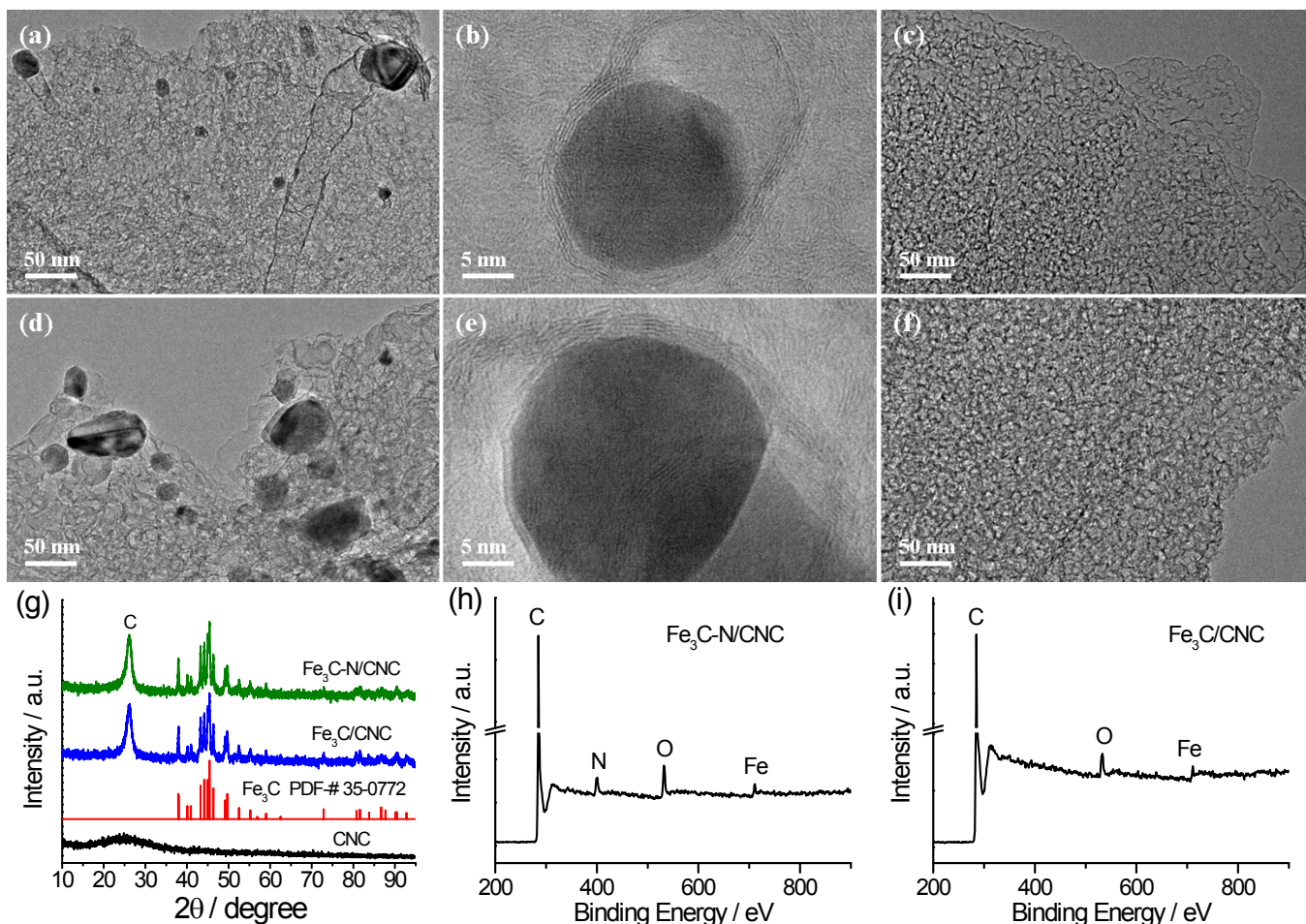


**Figure S5.** TEM image of (a,b) Fe<sub>3</sub>C-N/CNC, (c) N/CNC, (d,e) Fe<sub>3</sub>C/CNC, and (f) PMMA/CNC. (g) XRD patterns. Survey XPS spectra of (h) Fe<sub>3</sub>C-N/CNC and (i) Fe<sub>3</sub>C/CNC.

Fe<sub>3</sub>C nanoparticles exist in the Fe<sub>3</sub>C-N/CNC and Fe<sub>3</sub>C/CNC catalysts, similar to the cases in literatures,<sup>3</sup> and the control catalysts of N/CNC and PMMA/CNC present the similar morphology to CNC (Figure S5a-g). N species present in Fe<sub>3</sub>C-N/CNC but not in Fe<sub>3</sub>C/CNC (Figure S5h,i).

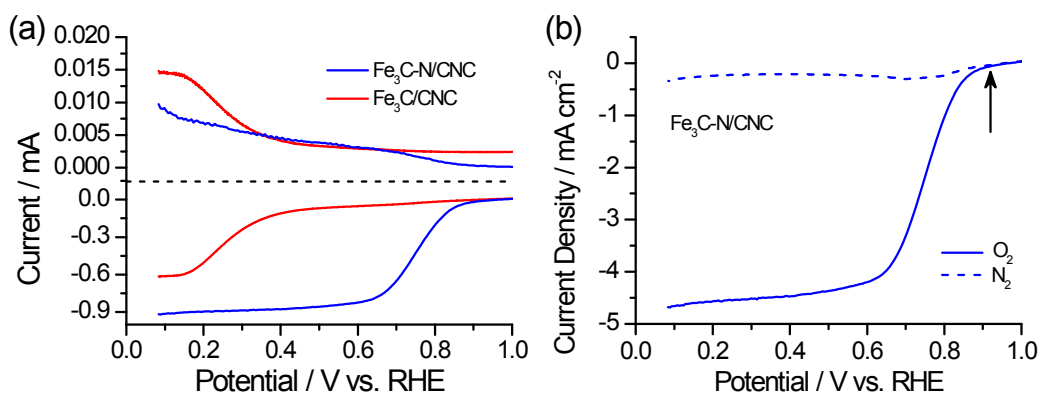


**Figure S6.** (a) RRDE curves of Fe<sub>3</sub>C-N/CNC and Fe<sub>3</sub>C/CNC. (b) RDE curves in O<sub>2</sub>- and N<sub>2</sub>-saturated solution.

Figure 4b in the main text is obtained based on the RRDE curves in Figure S6a.  $E_{on}$  is 0.920 V for Fe<sub>3</sub>C-N/CNC as arrowed in Figure S6b.

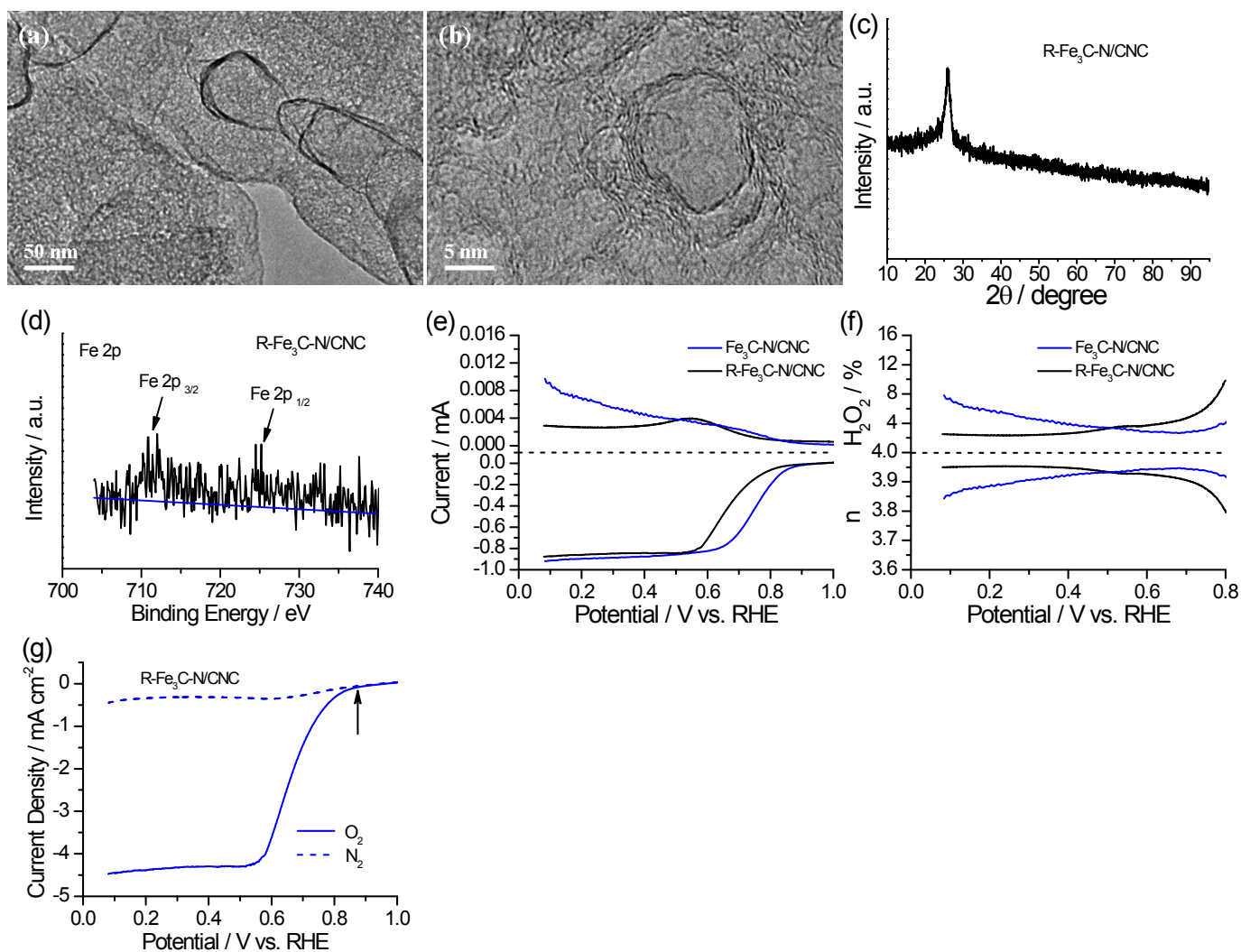


**Figure S7.** Characterizations of the  $\text{Fe}_3\text{C-N/CNC}$  after removing the  $\text{Fe}_3\text{C}$  nanoparticles by acid leaching in  $0.5 \text{ mol L}^{-1} \text{ H}_2\text{SO}_4$ , designated as  $\text{R-Fe}_3\text{C-N/CNC}$ . (a,b) TEM images. (c) XRD pattern. (d) Fe 2p spectrum. (e) RRDE curves. (f) Electron transfer number ( $n$ ) and  $\text{H}_2\text{O}_2$  yield at different potentials. (g) RDE curves in  $\text{O}_2$ - and  $\text{N}_2$ -saturated solutions. Note: In (e,f), the data for  $\text{Fe}_3\text{C-N/CNC}$  are also presented for comparison.

$\text{Fe}_3\text{C}$  nanoparticles could be removed by acid leaching while the Fe species is still present (Figure S7a-d). Electron transfer number ( $n$ ) and corresponding  $\text{H}_2\text{O}_2$  yield at different potentials indicate the  $\text{R-Fe}_3\text{C-N/CNC}$  catalyst still presents a dominant  $4e^-$  process (Figure S7e,f).  $E_{\text{on}}$  is  $0.876 \text{ V}$  (Figure S7g).

## ESI-6. Details in theoretical calculations

Theoretical models.

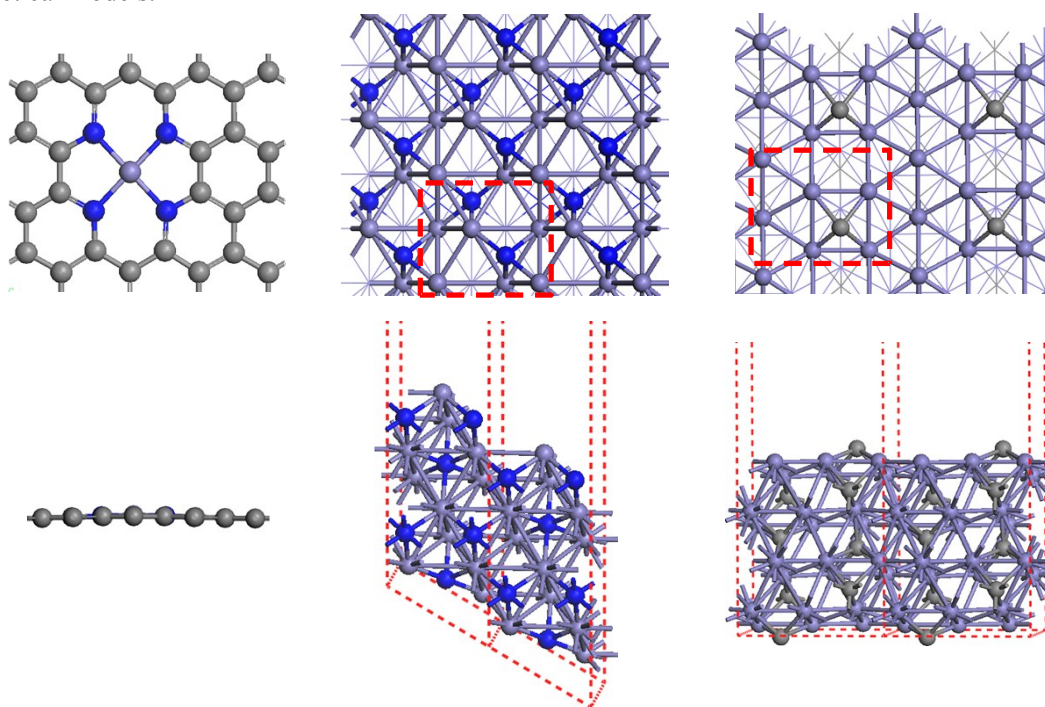


**Figure S8.** Models used for theoretical calculations in top (upper) and side (lower) views. (a) Fe-N<sub>4</sub>/C. (b) Fe<sub>2</sub>N. (c) Fe<sub>3</sub>C. C\_grey, N\_blue, Fe\_purple.

The graphitic Fe-N<sub>4</sub> structure was embedded in a 4×4 graphene supercell. The periodic slab model of Fe<sub>3</sub>C (001) was employed since it is a known low energy surface and has been used in surface catalysis modeling.<sup>4</sup> For Fe<sub>2</sub>N, a surface energy calculation was performed to determine the surface to be used. The results show that the surface energy of Fe<sub>2</sub>N (010) is lower than that of the Fe<sub>2</sub>N (100), Fe<sub>2</sub>N (001) and Fe<sub>2</sub>N (021) by 0.55, 0.80 and 2.15 eV per square nm, respectively. Therefore, the Fe<sub>2</sub>N (010) planes are preferentially exposed on the surface owing to the low surface energy, though they didn't show in XRD pattern due to the systematic extinction. Thus the periodic slab model of Fe<sub>2</sub>N (010) was chosen in this study. All the vacuum thicknesses were set to ~10 Å to minimize the interactions between adjacent images.

**Calculation details.** All calculations were performed with Vienna Ab-initio Simulation Package (VASP 5.2) at the spin-polarized DFT level.<sup>5</sup> The Perdew, Burke, and Ernzerhof (PBE) functional was employed to calculate the exchange and correlation energies, with a  $\sigma$  value of 0.05 eV for Methfessel-Paxton smearing.<sup>6</sup> All supercells were sampled with 4×4×1 Monkhorst-Pack k-point grids.

**Free energy diagram calculation.** The calculation of ORR free energy diagrams was performed according to the method proposed by Nørskov et al.<sup>7</sup> The free energy was calculated by the equation  $G = E + ZPE - TS$ , where E is the total energy, ZPE is the zero-point energy, T is the temperature in Kelvin and S is the entropy. The vibrational frequencies were calculated in the harmonic normal-mode approximation to determine ZPE and the entropy contributions (Table S2).

The free energy of ( $H^+ + e^-$ ) at the standard condition of pH = 0 and U = 0 is taken as 1/2H<sub>2</sub>. The free energy of O<sub>2</sub> was obtained from the reaction  $O_2 + 2H_2 \rightarrow 2H_2O$ , with a known free energy decrease of 4.92 eV. The free energy of H<sub>2</sub>O(l) was derived from  $G_{H_2O(l)} = G_{H_2O(g)} + RT \cdot \ln(p/p_0)$ , where R is the ideal gas constant, T = 298.15 K,  $p = 0.035$  bar, and  $p_0 = 1$  bar.

### ESI-7. The ORR process on the Fe-N<sub>4</sub>/C, Fe<sub>2</sub>N and Fe<sub>3</sub>C models

The 4e<sup>-</sup> ORR process in acidic medium is described by equations S1~S4 and illustrated by Figure S9. The asterisk (\*) indicates the adsorption sites or the species in chemisorbed state. The calculated free energy changes ( $\Delta G$ ) for each ORR step are denoted as  $\Delta G_1 \sim \Delta G_4$ , respectively.<sup>7</sup>

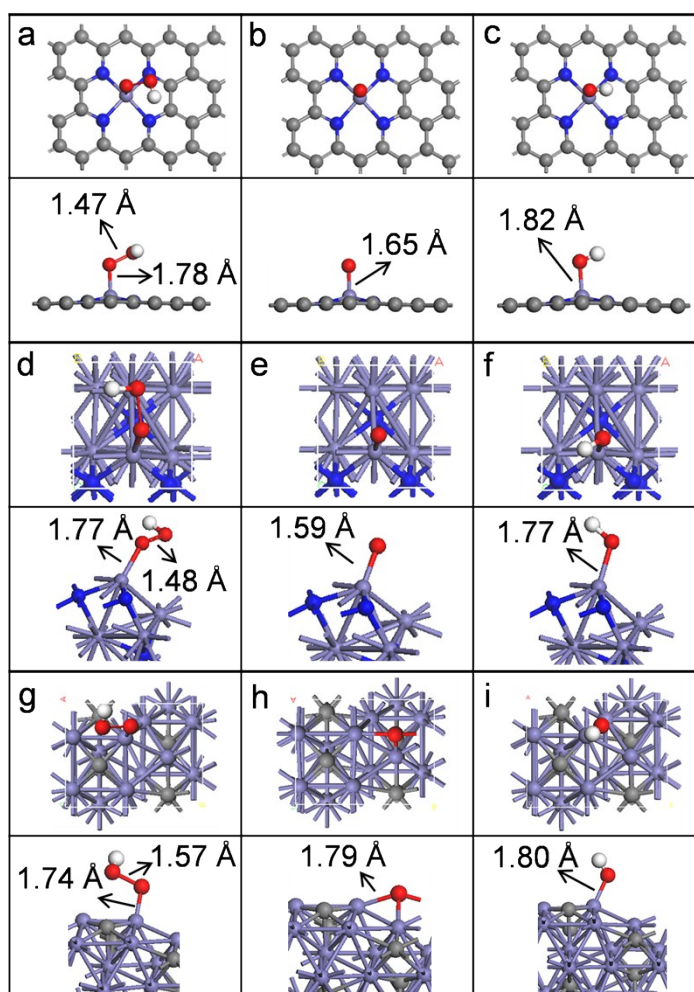
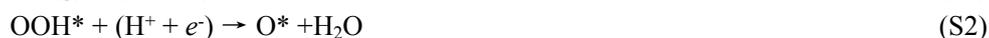


**Figure S9.** The ORR process on (a-c) Fe-N<sub>4</sub>/C, (d-f) Fe<sub>2</sub>N and (g-i) Fe<sub>3</sub>C in acidic medium, sketched in top (upper) and side (lower) views. For simplicity, some non-adsorbed H<sup>+</sup> and H<sub>2</sub>O are not plotted. The Fe-O and O-O bond length are marked accordingly. H\_ white, C\_ gray, N\_ blue, O\_ red, Fe\_ purple.

The calculation results are summarized in Tables S2&S3.

**Table S2.** Frequencies, zero-point energies and entropies of ORR intermediates

Model	Intermediate	Frequency (cm <sup>-1</sup> )	ZPE (eV)	Entropy (eV/T)
Fe-N <sub>4</sub> /C	O <sub>2</sub> *	1212.2, 462.5, 277.4, 204.4, 82.67, 69.9	0.1431	0.001498
	OOH*	3637.4, 1232.0, 705.4, 503.1, 246.6, 205.1, 164.9, 94.1, 76.8	0.4256	0.000820
	O*	766.3, 176.5, 157.7	0.0682	0.000597
	OH*	3676.8, 840.3, 524.5, 222.1, 143.9, 134.0	0.3435	0.000445
Fe <sub>2</sub> N	O <sub>2</sub> *	1197.4, 479.3, 337.6, 228.3, 143.6, 88.5	0.1534	0.003945
	OOH*	3560.4, 1271.0, 695.1, 450.6, 339.7, 277.2, 174.3, 122.8, 65.1	0.4312	0.004892
	O*	871.0, 177.9, 154.4	0.0746	0.004105
	OH*	3664.0, 682.7, 591.4, 213.7, 98.3, 35.8	0.3277	0.003269
Fe <sub>3</sub> C	O <sub>2</sub> *	632.5, 536.2, 432.2, 321.3, 238.4, 108.3	0.1407	0.000364
	OOH*	3629.9, 1128.1, 569.2, 278.8, 246.7, 169.0, 133.4, 103.7, 13.9	0.3889	0.002830
	O*	545.1, 227.7, 147.3	0.0570	0.000115
	OH*	3675.8, 660.3, 565.8, 255.6, 89.9, 54.7	0.3184	0.002926
/	H <sub>2</sub> O	3825.7, 3712.3, 1587.6, 109.5, 107.1, 49.5, 45.9, 33.4, 3.6	0.2936	0.001957 <sup>a</sup>
	H <sub>2</sub>	4299.9, 142.9, 140.0, 8.22, 3.16, 1.95	0.1092	0.001354 <sup>a</sup>
	O <sub>2</sub>	1557.3, 107.7, 92.9, 1.4, 1.1, 0.5,	0.1425	0.002126 <sup>a</sup>
	OOH	3513.0, 1245.0, 839.5, 270.9, 265.6, 110.2, 52.7, 11.6, 0.97	0.3911	0.002374 <sup>a</sup>

<sup>a</sup> The entropies of the species in gas phase were taken from the NIST database.<sup>8</sup>

**Table S3.**  $\Delta G$  for each ORR step (Unit: eV)

Models	$\Delta G_1$	$\Delta G_2$	$\Delta G_3$	$\Delta G_4$
Fe-N <sub>4</sub> /C	-1.631	-1.058	-0.580	-1.651
Fe <sub>2</sub> N	-2.040	-2.143	-0.223	-0.513
Fe <sub>3</sub> C	-2.272	-3.350	-0.083	<b>0.785</b>

For Fe-N<sub>4</sub>/C and Fe<sub>2</sub>N,  $\Delta G_3$  is the maximum among four steps, hence the step of O\* protonation to OH\* is likely the rate-limiting step around onset potential.<sup>7</sup>

For Fe<sub>3</sub>C, the step of the OH\* removal to form H<sub>2</sub>O shows the endothermic  $\Delta G_4$  of 0.785 eV, indicating the inert ORR activity.

## ESI-8. The theoretical ORR overpotentials of Fe-N<sub>4</sub>/C and Fe<sub>2</sub>N

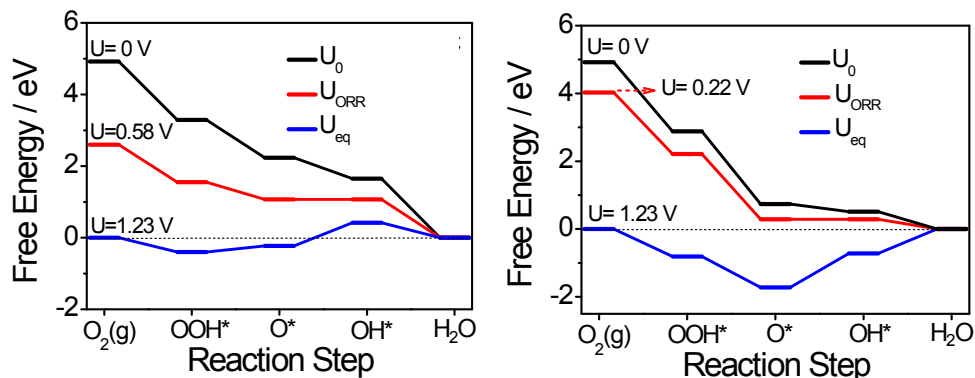


**Figure S10.** Free energy diagrams of the ORR on Fe-N<sub>4</sub>/C and Fe<sub>2</sub>N at applied potential ( $U$ ) of 0 V,  $U_{\text{ORR}}$ , and  $U_{\text{eq}}$ . Note:  $U_{\text{ORR}}$  corresponds to the thermodynamic onset potential at which all reaction steps are exothermic, and  $U_{\text{eq}}$  the equilibrium potential of 1.23 V.

The free energy ( $G$ ) at an applied potential ( $U$ ) is corrected by  $G(U) = G - neU$ , where  $e$  is the elementary charge and  $n$  is the number of transferred electrons. The theoretical ORR overpotential ( $\eta$ ) is calculated by the equation  $\eta = U_{\text{eq}} - U_{\text{ORR}}$ .<sup>9</sup> For Fe<sub>4</sub>-N/C and Fe<sub>2</sub>N,  $\eta$  is 0.65 and 1.01 V, respectively. Therefore, the theoretical results indicates the relative order of ORR activities should be Fe-N<sub>4</sub>/C  $\gg$  Fe<sub>2</sub>N  $\gg$  Fe<sub>3</sub>C, which is in high agreement with our experimental results, as shown in Figure S11.

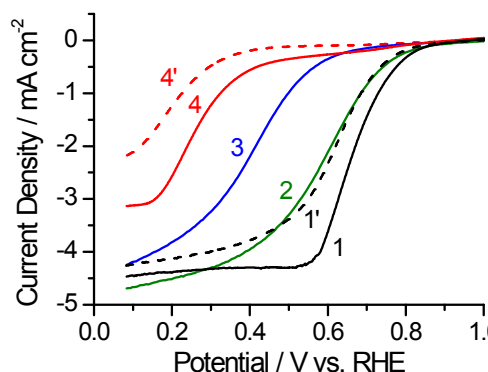


**Figure S11.** ORR activity comparison by RDE curves. 1, R-Fe<sub>3</sub>C-N/CNC (replotted from Figure S7); 2, R-Fe<sub>2</sub>N/NCNC (from Figure 2b); 3, Fe<sub>2</sub>N/CNC (from Figure 2b); 4, Fe<sub>3</sub>C/CNC (from Figure 4a). Note: The catalysts loading for plots 1', 2, 3 and 4' is 0.098 mg cm<sup>-2</sup>, and that for plots 1 and 4 is 0.400 mg cm<sup>-2</sup>.

Actually, #1 (#1') and #2 are the Fe/N/C with Fe-N<sub>x</sub>/C moieties ( $x \geq 4$ ), #3 is Fe<sub>2</sub>N, and #4 (#4') is Fe<sub>3</sub>C. Obviously, the relative order of ORR activity is Fe/N/C  $\gg$  Fe<sub>2</sub>N  $\gg$  Fe<sub>3</sub>C.

In addition, it indicates that the RDE curves for R-Fe<sub>3</sub>C-N/CNC and R-Fe<sub>2</sub>N/NCNC measured with the same catalyst (plots 1' and 2) loading are quite similar, which further reflect the same results: The excellent ORR activities of the Fe<sub>2</sub>N/NCNC and Fe<sub>3</sub>C-N/CNC catalysts with N source in preparation mainly originate from the Fe-N<sub>x</sub>/C moieties.

## References

- [1] (a) S. Chen, J. Y. Bi, Y. Zhao, L. J. Yang, C. Zhang, Y. W. Ma, Q. Wu, X. Z. Wang and Z. Hu, *Adv. Mater.* **2012**, *24*, 5593-5597; (b) K. Xie, X. T. Qin, X. Z. Wang, Y. N. Wang, H. S. Tao, Q. Wu, L. J. Yang and Z. Hu, *Adv. Mater.* **2012**, *24*, 347-352; (c) J. Zhao, H. W. Lai, Z. Y. Lyu, Y. F. Jiang, K. Xie, X. Z. Wang, Q. Wu, L. J. Yang, Z. Jin, Y. W. Ma,

- J. Liu and Z. Hu, *Adv. Mater.* **2015**, *27*, 3541-3545; (d) Z. Y. Lyu, D. Xu, L. J. Yang, R. C. Che, R. Feng, J. Zhao, Y. Li, Q. Wu, X. Z. Wang and Z. Hu, *Nano Energy* **2015**, *12*, 657-665.
- [2] (a) F. Jaouen, E. Proietti, M. Lefèvre, R. Chenitz, J. P. Dodelet, G. Wu, H. T. Chung, C. M. Johnston and P. Zelenay, *Energy Environ. Sci.* **2011**, *4*, 114-130; (b) G. Wu, K. L. More, C. M. Johnston and P. Zelenay, *Science* **2011**, *332*, 443-447; (c) J. Masa, W. Xia, M. Muhler and W. Schuhmann, *Angew. Chem. Int. Ed.* **2015**, *54*, 10102-10120; (d) G. Wu and P. Zelenay, *Acc. Chem. Res.* **2013**, *46*, 1878-1889; (e) Z. W. Chen, D. Higgins, A. P. Yu, L. Zhang and J. J. Zhang, *Energy Environ. Sci.* **2011**, *4*, 3167-3192.
- [3] (a) J. Wei, Y. Liang, Y. X. Hu, B. Kong, G. P. Simon, J. Zhang, S. P. Jiang and H. T. Wang, *Angew. Chem. Int. Ed.* **2016**, *55*, 1355-1359; (b) W. X. Yang, X. J. Liu, X. Y. Yue, J. B. Jia and S. J. Guo, *J. Am. Chem. Soc.* **2015**, *137*, 1436-1439; (c) Z. Y. Wu, X. X. Xu, B. C. Hu, H. W. Liang, Y. Lin, L. F. Chen and S. H. Yu, *Angew. Chem. Int. Ed.* **2015**, *54*, 8179-8183; (d) M. L. Xiao, J. B. Zhu, L. G. Feng, C. P. Liu and W. Xing, *Adv. Mater.* **2015**, *27*, 2521-2527; (e) Y. Hu, J. O. Jensen, W. Zhang, L. N. Cleemann, W. Xing, N. J. Bjerrum and Q. F. Li, *Angew. Chem. Int. Ed.* **2014**, *53*, 3675-3679; (f) G. Y. Ren, X. Y. Lu, Y. N. Li, Y. Zhu, L. M. Dai and L. Jiang, *ACS Appl. Mater. Interfaces* **2016**, *8*, 4118-4125; (g) S. Marzorati, J. M. Vasconcelos, J. Ding, M. Longhi and P. E. Colavita, *J. Mater. Chem. A* **2015**, *3*, 18920-18927.
- [4] C. F. Huo, Y. W. Li, J. G. Wang and H. J. Jiao, *J. Am. Chem. Soc.* **2009**, *131*, 14713-14721.
- [5] (a) G. Kresse and J. Hafner, *Phys. Rev. B* **1993**, *48*, 13115-13118; (b) G. Kresse and J. Furthmüller, *Phys. Rev. B* **1996**, *54*, 11169-11186; (c) G. Kresse and J. Hafner, *Phys. Rev. B* **1994**, *49*, 14251-14269; (d) G. Kresse and J. Furthmüller, *Comp. Mater. Sci.* **1996**, *6*, 15-50.
- [6] M. Methfessel and A. T. Paxton, *Phys. Rev. B* **1989**, *40*, 3616-3621.
- [7] J. K. Nørskov, J. Rossmeisl, A. Logadottir, L. Lindqvist, J. R. Kitchin, T. Bligaard and H. Jonsson, *J. Phys. Chem. B* **2004**, *108*, 17886-17892.
- [8] M. W. J. Chase, *NIST-JANAF Thermochemical Tables. Part 1, J. Phys. Chem. Ref. Data Monograph No. 9 (4th ed.)* American Chemical Society and American Physical Society, Washington, DC, **1998**.
- [9] (a) J. D. Baran, H. Grönbeck and A. Hellman, *J. Am. Chem. Soc.* **2014**, *136*, 1320-1326; (b) Y. Wang and H. P. Cheng, *J. Phys. Chem. C* **2013**, *117*, 2106-2112.